Numerical investigation on RC T-beams strengthened in the negative moment region using NSM FRP rods at various depth of embedment

Yanuar Haryanto[1,2a], Hsuan-Teh Hu[*1,3], Ay L. Han[4], Fu-Pei Hsiao[1,5],
Charng-Jen Teng[1], Banu A. Hidayat[1,4] and Laurencius Nugroho[1]

[1]*Department of Civil Engineering, College of Engineering, National Cheng Kung University,*
No. 1 University Road, Tainan, 701, Taiwan, ROC
[2]*Department of Civil Engineering, Faculty of Engineering, Jenderal Soedirman University,*
Jln. Mayjen. Sungkono KM 5, Blater, Purbalingga, 53371, Indonesia
[3]*Department of Civil and Disaster Prevention Engineering, College of Engineering and Science, National United University,*
No. 2, Lien Da, Nan Shih Li, Miaoli, 36063, Taiwan, ROC
[4]*Department of Civil Engineering, Faculty of Engineering, Universitas Diponegoro,*
Jln. Prof. Soedarto, Tembalang, Semarang, 50275, Indonesia
[5]*National Center for Research on Earthquake Engineering, 200 Sec. 3, Xinhai Road, Taipei, 10668, Taiwan, ROC*

Abstract. The application of Near Surface Mounted (NSM) method to strengthen reinforced concrete (RC) members in flexure through the use of Fiber Reinforced Polymer (FRP) rods has become a subject of interest to designers and researchers over the past few years. This technique has been extensively applied, and there is still a need for more experiments, analytical, and numerical studies to determine the effects of their parameters on the flexural performance of RC members. Therefore, a detailed 3D nonlinear finite element (FE) numerical model was developed in this study to predict the load-carrying capacity and the response of RC T-beams strengthened in the negative moment region accurately through the use of NSM FRP rods at different depth of embedment which are placed under three-point bending loading. The model was, however, designed with due consideration for the nonlinear constitutive material properties of concrete, yielding of steel reinforcement, NSM rods, and cohesive behaviors to simulate the contact between two neighboring materials. Moreover, the findings of the numerical simulations were compared with those from the experiments by other investigators which involve two specimens strengthened with NSM FRP rods added to one unstrengthened control specimen. The results, however, showed that the mid-span deflection responses of the predicted FE were in line with the corresponding data from the experiment for all the flexural loading stages. This was followed by the use of the validated FE models to analyze the effect of several properties of the FRP materials to provide more information than the limited experimental data available. It was discovered that the FE model developed is appropriate to be applied practically and economically with more focus on the parametric studies based on design to precisely model and analyze flexural negative moment strengthening for the RC members through the use of NSM FRP rods.

Keywords: finite element analysis; flexural strengthening; FRP rods; NSM reinforcement

1. Introduction

The provision of more strength for concrete structures during their service life is one of the essential difficulties facing structural engineers throughout the world. The strengthening is, however, required due to several reasons such as the increase in the magnitude of the loads to be applied, errors in the design and/or construction phase, corrosion and/or environmental damage, as well as aging (Tudjono *et al.* 2015, Haryanto *et al.* 2017a, Haryanto *et al.* 2017b, Haryanto *et al.* 2018, Haryanto *et al.* 2019, Hidayat *et al.* 2019, Haryanto *et al.* 2021a). Meanwhile, the rehabilitation of the deteriorated structures can be achieved through the use of different methods such as steel or concrete jackets (Chen and Tseng 2001, Aldhafairi *et al.* 2020, Hwang *et al.* 2020, Zhang *et al.* 2018, Attar *et al.* 2020), external post-tensioning (Tan 2014, Lee *et al.* 2018), section enlargement (Nuroji *et al.* 2020), externally-bonded (EB) steel plates (Alam *et al.* 2014) as well as the replacement of degraded members or the addition of extra members (Kaplan *et al.* 2011). These traditional repair methods have the ability to improve the strength capacity and stiffness of deficient concrete structures but they also increase the dead load and require more time. Therefore, there is a need to search for other alternative methods and materials to achieve more efficient results.

The strengthening of structural members externally was initiated in 1949 (Asplund) through the concept of grouted or embedded reinforcement which involves the use of external steel bars to improve the strength of the bridge girders in flexure. Several studies have focused on the strengthening of reinforced concrete (RC) structures using externally bonded Fiber Reinforced Polymer (FRP) laminates and fabric sheets over the past 20 years

*Corresponding author, Professor
E-mail: hthu@mail.ncku.edu.tw
[a]Associate Professor
E-mail: yanuar.haryanto@unsoed.ac.id

(Sherwood and Soudki 2000, Täljsten and Elfgren 2000, Hu *et al.* 2004, Al-Saidy *et al.* 2010, Xue *et al.* 2010, Lesmana *et at.* 2013, Lin *et al.* 2014, Salma *et al.* 2019, Nie *et al.* 2020). This technology has been applied to different practical projects throughout the world. In recent times, the techniques of Near Surface Mounted (NSM) FRP reinforcement have been developed and practically implemented, thereby, leading to several comprehensive studies on the concept as observed in the experimental (Sharaky *et al.* 2013, Al-Bayati *et al.* 2016, Sabau *et al.* 2018, Wang *et al.* 2019, Barris *et al.* 2020), numerical (Hawileh 2012, Zhang and Teng 2014, Sharaky *et al.* 2017, Sharaky *et al.* 2018, Firmo *et al.* 2018, Chellapandian *et al.* 2019, Al-Abdwais and Al-Mahaidi 2020, Almassri and Halahla 2020, Stoner and Polak 2020), and analytical (Shakary *et al.* 2015, Yang *et al.* 2019, Chen *et al.* 2019, Abdallah *et al.* 2020) studies of the past few years with the findings showing its effectiveness in causing an increment in the flexural and shear capacities in RC structural members' behavior.

The method of NSM is established on the bonding of FRP bars, laminates, or fabrics into pre-cut grooves of the cover of a concrete. It is possible to place these grooves in the RC members' tensile surfaces for flexure reinforcement, beams sides for shear reinforcement, or along the columns heights as required. Pavin and Shah (2016) and Al-Saadi *et al.* (2019) critically reviewed previous studies on applying NSM FRP to structural members with the system reported to have several advantages over NSM steel as observed from its fatigue and corrosion resistance, high strength to weight ratio, durability, low density as well as the ease with which it can be shaped and installed. Moreover, it also has certain major advantages compared to the conventional externally-bonded FRP systems (De Lorenzis and Teng 2007) and these include (1) convenient and minimum time of installation on site, (2) more effective bonding to the substrate concrete based on its full embedment in adhesives, and (3) protection from natural disasters using concrete cover and less exposure to inadvertent damages. Meanwhile, its performance is mainly affected by the materials used for bonding, the interaction of bond between the filling material and NSM bar, bond between concrete interface and filling material, groove size and its location from the edges (De Lorenzis and Teng 2007). Recently, Deng *et al.* (2021a) investigated the flexural behavior of reinforced concrete (RC) beams strengthened with near-surface mounted (NSM) carbon fiber reinforced polymer prestressed concrete prisms (CFRP-PCPs), and found that the strengthened beams showed a higher first-cracking, yielding, and ultimate load as the bond length and prestress level of CFRP-PCPs increased up to a critical level. In addition, an experimental study of the shear performance of RC beams strengthened with NSM CFRP-PCPs showed that the shear capacity and deformation were enhanced with the increase of prestressing levels of CFRP rods and the decrease of CFRP-PCPs spacing (Deng *et al.* 2021b).

FRP rods are, however, produced in different types which ranged between simple smooth and those treated and this is majorly due to the lack of firm standards. Meanwhile, the main processes developed for the improvement of bond

behavior are categorized into two which are (1) outer surface deformation including ribbed, indented, and braided rods and (2) surface treatments such as sand grain-covered and epoxy coated rods (Cosezna *et al.* 1997). Cosezna *et al.* (1997) comprehensively reviewed studies on the bond behavior for several FRP rod reinforcement types in concrete in order to determine the bond between the rods and concrete. FRP bars that have efficient surface conditions were found to have the ability of achieving average bond stress which is the same as steel bars (Cosezna *et al.* 1997).

The embedded depth of the FRP rods affects the bond between the rod and the epoxy resin as well as between epoxy resin and concrete. The rods' position relative to the concrete surface is another factor influencing stress distribution in concrete (Budipriyanto *et al.* 2018). Moreover, the experimental research by Sapulete (2018) showed that the FRP rods implemented in line with the code ACI 440.2R-08 (2008) produced an 83% capacity improvement as well as a substantial enhancement for the ductility in comparison with members without external reinforcement. Finally, the mounting of FRP rods using only half of its area also has the ability to cause an increment at the moment carrying capacity of the member by 37%. Meanwhile, the ductility of the members was observed not to have improved substantially and without any pattern of yielding was noticed after yielding in conventional steel. It is, however, possible to use the half-embedded FRP rods practically with due consideration for the manufacturer's description in applying the bonding agent to the rods.

NSM systems have been comprehensively applied but there is still a need for further investigation experimentally, analytically, and numerically to determine the effects of its strengthening parameters on RC members' flexural performance. This research was, therefore, conducted to numerically develop a detailed 3D nonlinear finite element (FE) model with the ability to predict the load-carrying capacity and response of RC T-beams strengthened in the negative moment region. This involved the use of NSM FRP rods at different embedment depth under three-point bending loading through the help of the FE code ABAQUS (2011). The provision of more strength to concrete members in the negative moment region has been observed to provide greater attention in comparison with the positive region. Meanwhile, some physical challenges related to the application of strengthening in this region for a continuous span which is a vital zone based on the availability of significant shear and moments in similar area has been addressed by Jumaat *et al.* (2010). The availability of the columns in these areas forbids applying strengthening system on the beam's web portion (Al-Khafaji and Salim 2020).

Another important aspect for consideration is the difference in the depth of embedment as observed in the frequent cases encountered by engineers concerning the inability to meet the standard required by ACI 440.2R-08 (2008) for fields and structural frames of buildings (Sapulete 2018). The developed FE models have been confirmed to be effective through the comparison of its

(a) Test setup and measuring instruments

(b) Specimen details and FRP rod placement
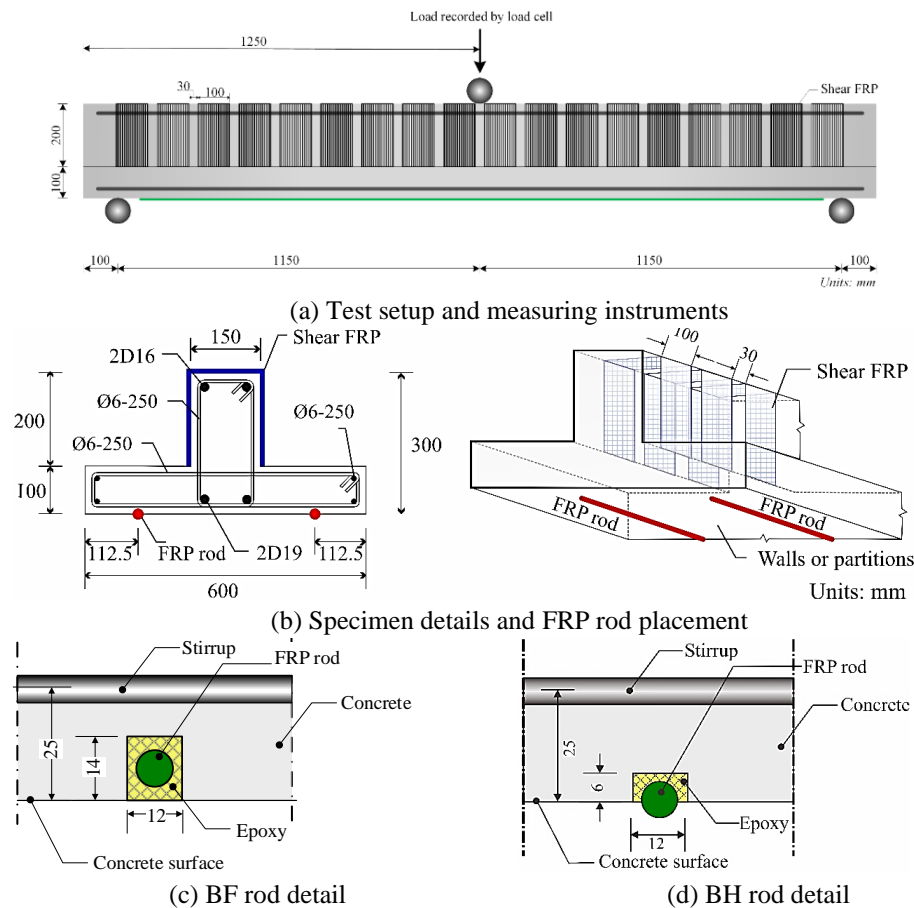

(c) BF rod detail   (d) BH rod detail

Fig. 1 Experimental setup and beams detail (Sapulete 2018, Haryanto *et al.* 2021b)

predicted load and midspan deflection with experimental data in Sapulete (2018). It was also used to numerically determine the influence of FRP material properties on the response of RC T-beams strengthened in the negative moment region. Therefore, this research showed the finite element method is practical and valid to model RC T-beams strengthened in the negative moment region using NSM FRP rods at various depth of embedment.

2. Experimental setup

This numerical analysis conducted was founded on the experimental research by Sapulete (2018) to evaluate the response of the RC T-beams which were strengthened using NSM FRP rods considering different embedment depth in the negative moment region under a three-point bending or one-point loading which was monotonously increased until the specimen failed. The research involved the use of two strengthened RC T-beams as well as an unstrengthened specimen which was applied as the control (BM) with the beams having a total length of 2500 mm while the total height of the T-section was 300 mm, web-width was 150 mm, flange-width at 600 mm, and the flange-depth at 100 mm. Moreover, the ribbed steel reinforcement had two bars with 19 mm diameter in the zone of tension which was tagged bottom reinforcement, another two with 16 mm diameter in the zone of compression tagged the top

reinforcement while steel stirrups with 6 mm diameter and spaced by 250 mm were applied as shear reinforcement, all in accordance with the code SNI 2052 (2017). Meanwhile, one of the two beams was strengthened with two 8 mm-diameter FRP rods using an embedment depth stated by the code (BF) while the remaining beams were strengthened using FRP rods with the same properties but embedded only half of its area (BH). Furthermore, the FRP sheets applied for shear strengthening were installed along the entire span of the strengthened beam at 100 mm width and spaced at 130 mm. The detailed setup and the loads applied to the beams tested are indicated in a schematic manner as shown in Fig. 1 while the complete experiment and factors have been described by Sapulete (2018).

As in the experiment research by Sapulete (2018), the beams were all simply supported and subjected to a monotonic, increment deflection until failure. To detect the occurrence of buckling, two LVDTs (SD 100-C) with a sensitivity of 50×10^{-6} strain/mm were used to monitor the vertical deflection of the beam, while three LVDTs were used to measure the horizontal deformation of the beam. The load response was measured by a load cell. A one-point loading system was used to simulate a maximum bending moment in combination with a maximum shear at the mid-point (Tudjono *et al.* 2017, Tudjono *et al.* 2018). To simulate a negative bending moment in the slab, the beam was turned upside down, as the load was induced with the help of a hydraulic jack that produced a downwards force.

The beam was tested with a deflection increment of 0.144 mm/sec, and the data was recorded by the data logger (TDS-630), which was connected to a computer using the TDS-7130 software.

3. Finite element (FE) modelling

3.1 Description of the elements

The simulation of the concrete was conducted with a three-dimensional composite solid element (C3D8R) which is a solid brick element with 8 nodes having three translation degrees of freedom in each node at x, y, and z directions and observed to be suitable to model the concrete's nonlinear behavior due to its ability to crack in tension at three orthogonal directions, crush under compression, and ensure plastic deformation and creep. Meanwhile, the FRP rod was modeled using the same C3D8R element while the FRP sheet was by 4-noded linear elastic S4R shell element which is three-dimensional and has membrane or in-plane stiffness without bending or out-of-plane stiffness, and three degrees of freedom in each node also at x, y, and z directions. It also has a varying thickness, significant deflection, stress tightening, and a cloth option used for a tension-only behavior. This non-linear option behaved like a cloth such that tension loads were supported but compression loads caused the element to wrinkle. Furthermore, two-noded deformable truss elements having three-degrees of freedom with translations in x, y, and z global coordinate directions at each node (T3D2) were applied to simulate all the reinforcing bars.

Steel reinforcements were embedded completely in the concrete materials and a perfect bond was assumed between the steel and surrounding concrete to simplify the modeling of such behavior. This assumption ignored the slip and shear stresses developed between the embedded reinforcement and surrounding materials. Moreover, the FRP sheets were created as a skin on the part of the concrete and this means there is complete bond between them. Therefore, no relationship was set between the FRP sheets and concrete since it was not needed but a contact interaction was modeled between the surrounding materials and FRP rod based on cohesive behavior with elastic response explained using an uncoupled traction-relative displacement law and the three traction stresses considered are presented in Eq. (1).

$$\begin{pmatrix} t_n \\ t_s \\ t_t \end{pmatrix} = \begin{bmatrix} K_{nn} & 0 & 0 \\ 0 & K_{ss} & 0 \\ 0 & 0 & K_{tt} \end{bmatrix} \begin{Bmatrix} u_n \\ u_s \\ u_t \end{Bmatrix} \qquad (1)$$

where t_n, t_s, and t_t (all in N/mm²) indicate normal and two shear traction stress components, respectively, u_n, u_s, and u_n (all in mm) represents the corresponding separations while K_{nn}, K_{ss}, and K_{tt} (all in N/mm³) are the penalty stiffness parameters. Table 1 summarizes the penalty stiffness parameters determined for the simulation based on the previous study by Haryanto *et al.* (2021c).

3.2 Geometry of the developed FE models

Table 1 Penalty stiffness variables for FE models

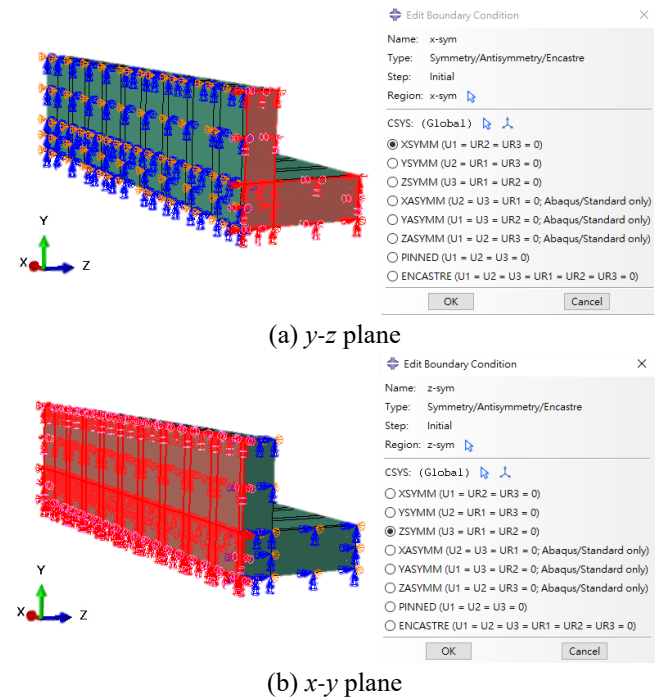| Specimen	K_{ss} (N/mm³)	K_{tt} (N/mm³)	K_{nn} (N/mm³)
BH	8	8	3000
BF	3.5	3.5	3000

(a) *y-z* plane

(b) *x-y* plane

Fig. 2 Symmetry conditions of the models

Similar dimensions, properties of materials, boundary conditions, and geometry were used for the models developed for the simply-supported beam specimens which were tested. Moreover, only ¼ of the beams were designed in the model to have symmetrical boundary conditions in two planes based on the symmetry of the geometry, loadings, and boundary conditions. This decision was favorable due to the decrease in the elements' number by four and this further saved the time for computations. The symmetry was simulated by holding the displacement in the plane perpendicular to its plane (Fig. 2). The FE models developed in this study had the same notation as those obtained from the research conducted using experiments. An example of the models developed for the beams strengthened by placing the NSM FRP rod along the entire length is presented in Fig. 3(a) while the sectional detail of each model is indicated in Fig. 3(b). Meanwhile, the meshed FE model for the strengthened specimen is depicted in Fig. 3(c).

3.3 Properties of the materials

A nonlinear stress-strain model represented with Eq. (2) through (4) which was proposed by Hsu and Hsu (1994) was applied to the uniaxial concrete behavior in compression. It considered the effects of lateral steel or shear stirrups in confining the concrete and was based on the physically important variables which are determinable using experiments and has the ability to represent both
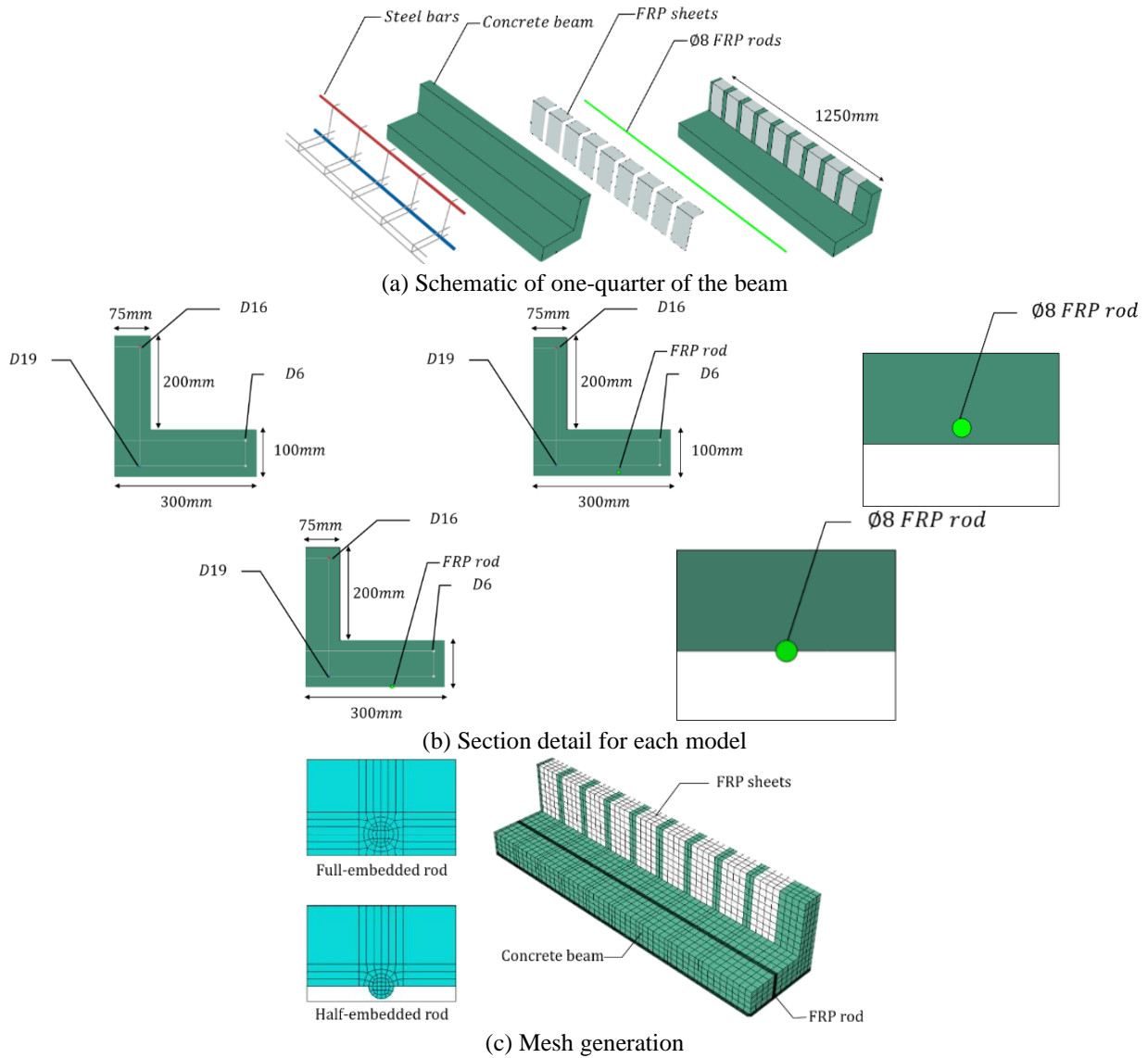
(a) Schematic of one-quarter of the beam

(b) Section detail for each model

(c) Mesh generation

Fig. 3 Detail of FE models

ascending and descending branches of the curve.

$$\sigma_c = \left(\frac{\beta (\varepsilon_c / \varepsilon_0)}{\beta - 1 + (\varepsilon_c / \varepsilon_0)^{\beta}} \right) \sigma_{cu} \tag{2}$$

$$\beta = \frac{1}{1 - (\sigma_{cu} / \varepsilon_0 E_c)} \tag{3}$$

$$\varepsilon_0 = 8.9 \times 10^{-5} \sigma_{cu} + 2.114 \times 10^3 \tag{4}$$

where, the σ_c is the compressive stress value after the yield point (at $0.5\,\sigma_{cu}$) and the descending portion (to $0.3\sigma_{cu}$), and ε_0 is the strain at σ_{cu}. The units used are kips/in² (1 MPa = 0.145037743 kips/in²). Meanwhile, the damaged parameters for the concrete were calculated using Eq. (5).

$$d_c = \frac{(1 - \eta_c)\varepsilon_c^{\square in} E_0}{\sigma_c + (1 - \eta_c)\varepsilon_c^{\square in} E_0} \; ; \; d_t = \frac{(1 - \eta_t)\varepsilon_t^{\square ck} E_0}{\sigma_c + (1 - \eta_t)\varepsilon_c^{\square ck} E_0} \tag{5}$$

where η_c and η_t are the ratio of plastic strain to inelastic or cracking strain and were suggested to be 0.6 and 0.9 respectively by Wei *et al.* (2014).

The average cylindrical concrete compressive strength obtained was 36.29 MPa while the Poisson's ratio was set at 0.2. Meanwhile, Eqs. (6) and (7) were used to calculate the modulus of elasticity and tensile strength of the concrete in line with the ACI 318-14 code (2014) but reduced with Taiwanese code in designing the concrete structure (Construction Agency 2019).

$$E_c = 0.8 \times 4700 \sqrt{f_c'} = 3760 \sqrt{f_c'} \tag{6}$$

$$f_t' = 0.75 \times 0.33 \sqrt{f_c'} = 0.25 \sqrt{f_c'} \tag{7}$$

The applications of these equations and constitutive models on the 36.29 MPa strength concrete used in the model produced the concrete stress-strain relationships presented in Fig. 4.

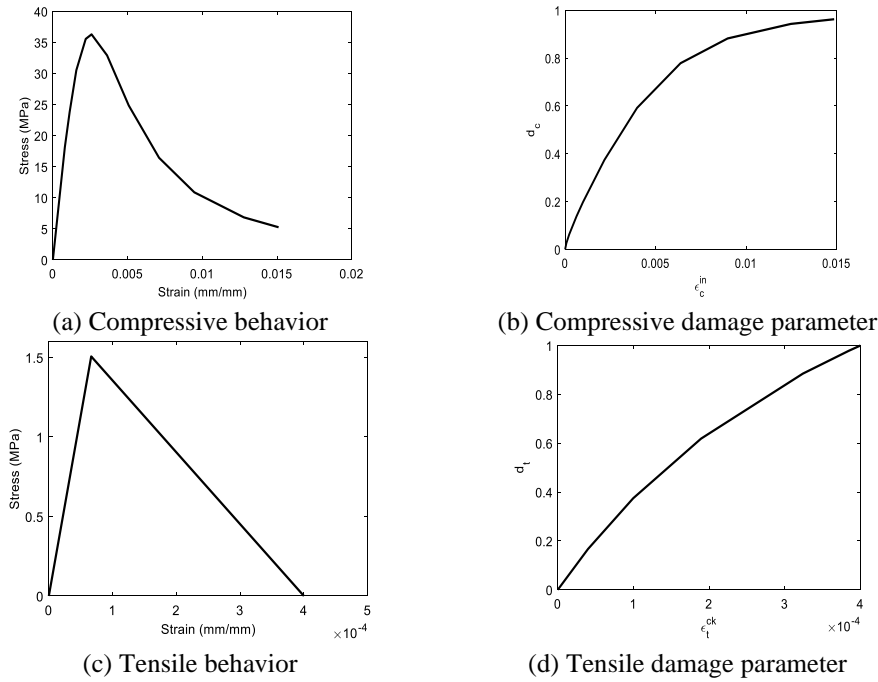The two sections of the uniaxial stress-strain behavior

(a) Compressive behavior

(b) Compressive damage parameter

(c) Tensile behavior

(d) Tensile damage parameter

Fig. 4 Concrete stress-strain curve

Table 2 Properties of the material for steel reinforcement

No.	Diameter (mm)	Cross-sectional area (mm^2)	Density (ton/mm^3)	Yield strength (MPa)
D6	6	28.274		371.04
D16	16	201.062	7.85×10^{-9}	402.18
D19	19	283.539		407.90

Table 3 Material properties for FRP sheet

Properties	Description	Value	Unit
E_{11}	Young's modulus along the fiber direction	225	GPa
E_{22}	Young's modulus perpendicular to the fiber direction	16.28	GPa
G_{12}	Shear modulus	4.31	GPa
X_1^T	Tensile strength in the fiber direction	3850	MPa
X_1^C	Compressive strength in the fiber direction	-2369.23	MPa
X_2^T	Tensile strength perpendicular to the fiber direction	109.58	MPa
X_2^C	Compressive strength perpendicular to the fiber direction	-286.28	MPa
S_{12}	Shear strength	118.46	MPa
S_{6666}	Nonlinear shear parameter	4.64 e-25	Pa^{-3}

for the concrete in tension were indicated and the first involved the presentation of a linear elastic behavior to the tensile strength, f_t, while the second was initiated with cracking and how it was propagated in the material of the concrete under tension which was indicated with a descending branch in the figure. The modeling of this phase behavior was through the application of a softening method which involved implementing stress-strain relationships which were linear, bilinear, or nonlinear (Belarbi and Hsu, 1994). Moreover, a linear behavior was used with the ultimate cracking strain assumed to be 0.004 while the minimum tensile stress was set close to zero to avoid the potential convergence problem in the modeling process.

The nonlinear response of the steel reinforcement bars was assumed to be linear elastic-perfectly plastic while the Poisson's ratio was made to be 0.3 and the elastic modulus was 200 GPa. The properties of the steel reinforcement used for simulation are, however, indicated in Table 2.

FRP rod mechanical properties were obtained from the PT. SIKA Indonesia with the modulus of elasticity and tensile strength recorded to be 148 GPa and 3100 MPa, respectively. Meanwhile, it was only the modulus in fiber direction E_{11} and the tensile strength in fiber direction X_1^T which were provided for the FRP sheet by PT. SIKA Indonesia while other properties were in line with the TB-06-CRP-1 (2007) as shown in Table 3. Moreover, a subroutine known as UMAT in ABAQUS which allows users to write their constitutive material model was applied

in the Tsai-Wu theory (Tsai and Wu 1971) to define the failure behavior of FRP sheet in the simulation. Finally, the Poisson's ratio for FRP was set at 0.3 while FRP nonlinear response was assumed to be linearly elastic.

4. Results and discussion

4.1 The relationship between the results of numerical simulation and experiment

The findings of the FE numerical simulations obtained from this study and the experiments of Sapulete (2018) were compared to analyze the FE model developed and determine whether it is valid. The experimentally recorded and numerically simulated load-midspan deflection of the control and two negative moment region strengthened RC T-beams with NSM FRP rods were compared and presented in Fig. 5. A reasonable agreement was, therefore, observed
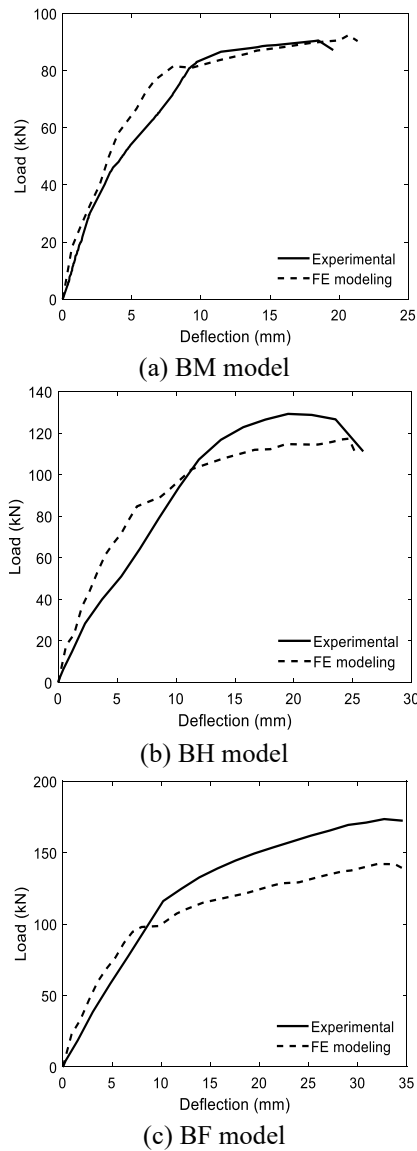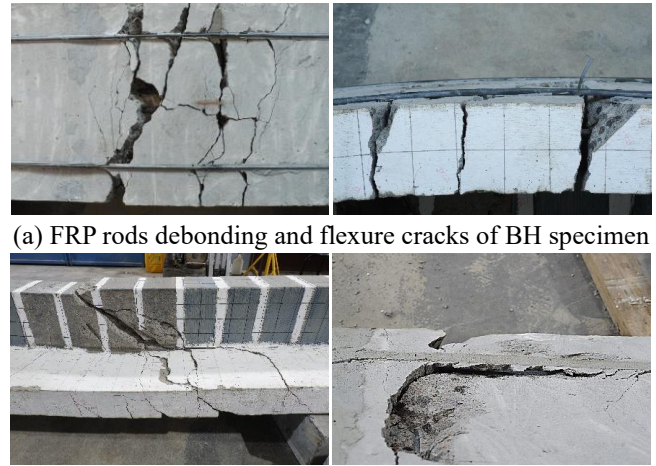
(a) BM model

(b) BH model

(c) BF model

Fig. 5 Experimental measurements and FE simulation comparison

(a) FRP rods debonding and flexure cracks of BH specimen

(b) Shear-flexure cracks and concrete interface failure at the rods of BF specimen

Fig. 6 Failure mode of BH and BF (Sapulete 2018)

Table 4 Experimental results and predicted FE analysis comparison

Specimen	Load, P_u (kN)		Deflection, δ_u (mm)	
	Experimental	Numerical	Experimental	Numerical
BM	90.54	92.39	18.49	20.67
BH	129.23	117.31	19.50	24.67
BF	173.51	142.07	32.69	32.00

between the two findings at all stages of loading up to the time all the specimens failed.

Similarly with Sapulete *et al.* (2018), it was observed that the control beam (BM) failed as an under-reinforced member. The first crack in the concrete's tension area occurred at a loading level of 30% of the ultimate load, while the reinforced steel yielded at a loading level of 96% of the ultimate strength. Owing to significant shifting of the neutral axis towards the compression zone, the strains in the concrete fibers reached its failure-strain limit and the member failed due to the crushing load of concrete in the compression area. The member underwent large deformations from the prolonged yielding of the steel bars, resulting in a post peak curve. The beam BH with the half-embedded FRP rods and BF with the fully-embedded FRP rods behave almost identically. The concrete in tension cracked at levels of 32% (BH) and 43% (BF) of their ultimate load. The significant difference in behavior observed after the yielding was that the BH could only carry

an additional 37% of the ultimate load of beam BM, whereas BF had an 82% capacity increase.

Furthermore, Sapulete (2018) stated that FRP sheets confinement has slightly effect on BH specimen since it was collapses due to FRP rods debonding, thereby making the beam more ductile. The beam demonstrated severe flexure cracks at the mid-point (Fig. 6(a)). In contrast, BF specimen showed that the concrete material did not crush when it reached the ultimate strain value of 0.003. This condition is influenced by the confinement of the FRP sheets on the concrete in the compression area. BF was characterized by shear-flexure failure and large diagonal cracks that propagated from the tensile fibers of the concrete at and around the mid-point up till the compression zone (Fig. 6(b)). Finally, the values for ultimate load and corresponding deflection were also compared for the predicted and experimented studies and the results are presented in Table 4 where the normalized mean square error (NMSE) for the ultimate load as well as the corresponding deflection were found to be 0.024 and 0.017 respectively for all the specimens.

4.2 Analytical approach

The ultimate load, P_u, for the strengthened beams obtained from the experiment and numerical analysis were compared with the analytical model from ACI 318-14 (2014) as indicated in Fig. 7. The comparison was, however, made by assuming the plane sections are still plain after they have been loaded, a perfect bond exists between steel reinforcement and substrate of the concrete,
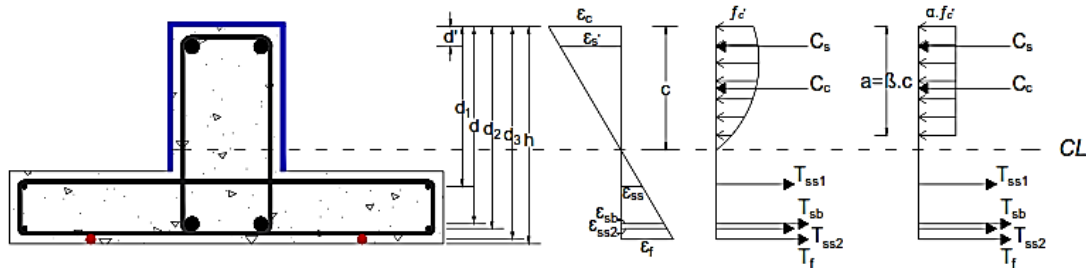
Fig. 7 Theoretical model at the ultimate stage

the concrete's ultimate compressive strain is 0.003, FRP behaves linearly elastic, and steel reinforcement behaves elastic-perfectly plastic. It should be noted that the analytical approach did not take FRP sheets into consideration.

Effective concrete strain (ε_c), steel reinforcement strains ($\varepsilon_{ss1}, \varepsilon_{ss2}, \varepsilon_{sb}, \varepsilon_s'$), and FRP rod strain ($\varepsilon_f$) are calculated using Eq. (8) in line with the strain compatibility

$$\frac{\varepsilon_f}{d_3 - c} = \frac{\varepsilon_{ss2}}{d_2 - c} = \frac{\varepsilon_{sb}}{d - c} = \frac{\varepsilon_{ss1}}{d_1 - c} = \frac{\varepsilon_s'}{c - d'} = \frac{\varepsilon_c}{c} \quad (8)$$

where d (mm) is distance between the beam top and main steel reinforcement, d' (mm) is distance between the beam top and top steel reinforcement, d_1 (mm) is distance between the beam top and upper layer of flange steel reinforcement, d_2 (mm) is distance between the beam top and lower layer of flange steel reinforcement, d_3 (mm) is distance between the beam top and FPR reinforcement, and c (mm) is neutral axis depth from the top. The equilibrium of internal forces was fulfilled using Eqs. (9) to (15)

$$C_c + C_s = T_{ss1} + T_{sb} + T_{ss2} + T_f \quad (9)$$

$$C_c = \alpha f_c' \beta c b \quad (10)$$

$$C_s = A_s' E_s \varepsilon_s' \quad (11)$$

$$T_{ss1} = A_{ss1} f_{yss1} \quad (12)$$

$$T_{sb} = A_{sb} f_{ysb} \quad (13)$$

$$T_{ss2} = A_{ss2} f_{yss2} \quad (14)$$

$$T_f = A_f E_f \varepsilon_f \quad (15)$$

where T_{ss1}, T_{sb}, T_{ss2} (N) are steel reinforcement tension forces, T_f (N) is FRP reinforcement tension force, C_c (N) is concrete compression force, C_s (N) is steel reinforcement compression force, A_{sb} (mm²) is main steel reinforcement cross-sectional area, A_s' (mm²) is top steel reinforcement cross-sectional area, A_{ss1} and A_{ss2} (mm²) are flange steel reinforcement cross-sectional area, A_f (mm²) is FRP rod cross-sectional area, ε_s' is top steel reinforcement strain, ε_f is FRP reinforcement strain, and E_f (MPa) is FRP reinforcement elastic modulus. The stress block parameters α and β are equal to 0.85 according to the ACI 318-14.

The beam's ultimate flexural moment M_u (Nmm) was later determined using Eqs. (16) to (22) as follows where
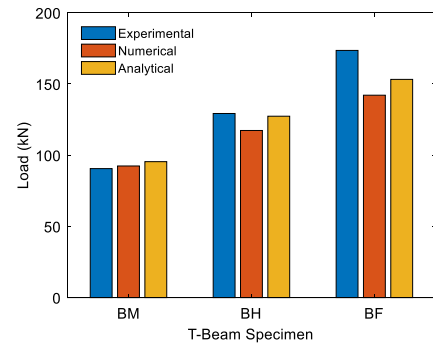

Fig. 8 Summary of different methods of investigation

$$M_u = M_c + M_{s'} + M_{ss1} + M_{sb} + M_{ss2} + M_f \quad (16)$$

$$M_c = Cc \left(c - \frac{\beta c}{2} \right) \quad (17)$$

$$M_s = C_s (c - d') \quad (18)$$

$$M_{ss1} = T_{ss1}(d_1 - c) \quad (19)$$

$$M_{sb} = T_{sb}(d - c) \quad (20)$$

$$M_{ss2} = T_{ss2}(d_2 - c) \quad (21)$$

$$M_f = T_f(d_3 - c) \quad (22)$$

M_c (Nmm) is concrete moment contribution, M_s (Nmm) is top steel reinforcement moment contribution, M_{ss1} (Nmm) is upper layer of flange steel reinforcement moment contribution, M_{sb} (Nmm) is main steel reinforcement moment contribution, M_{ss2} (Nmm) is lower layer of flange steel reinforcement moment contribution, and M_f (Nmm) is FRP reinforcement moment contribution. The analytical ultimate load-carrying capacity P_{u-th} (kN) was later calculated using the following Eq. (23).

$$P_{u-th} = \frac{4M_u}{l} \times 10^{-3} \quad (23)$$

where l is clear span of the beam which was 2300 mm.
A reasonable agreement was obtained for all the specimens between experimental, numerical, and analytical ultimate load results for RC T-beams strengthened using NSM FRP rods in the negative moment region. The values from the analytical approach were discovered to be relatively under-predicted and tend towards the numerical values in comparison with the experimental findings as indicated in Fig. 8. The analytical evaluation also showed BM only had
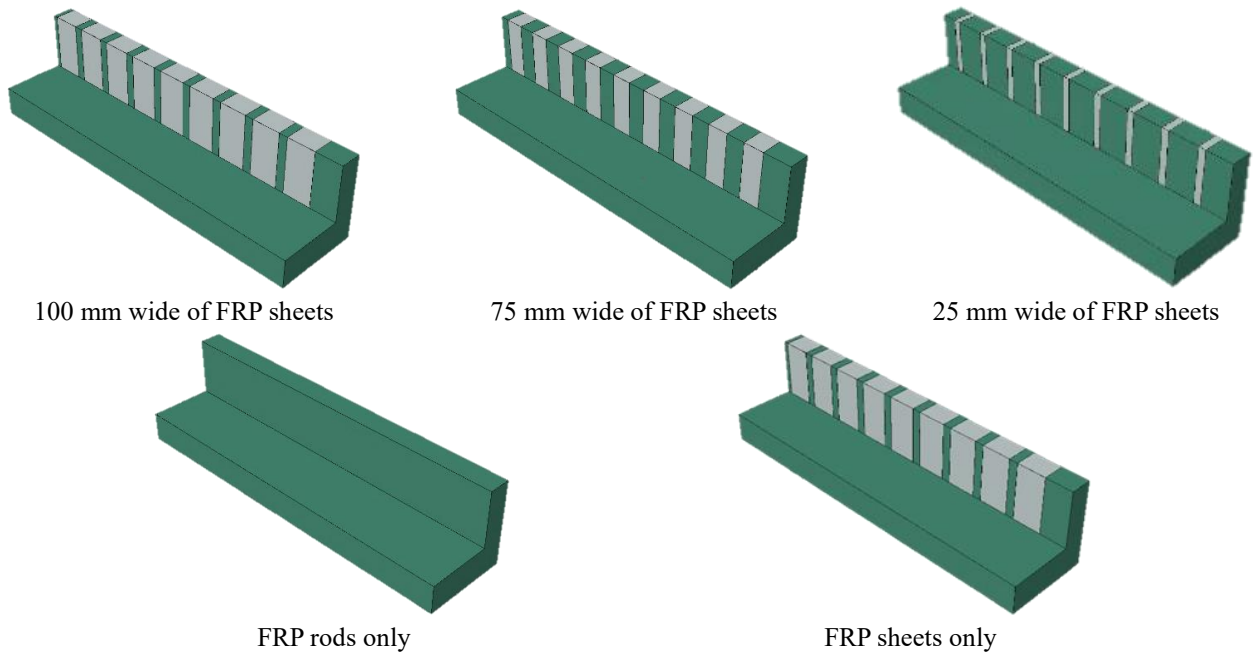
100 mm wide of FRP sheets   75 mm wide of FRP sheets   25 mm wide of FRP sheets

FRP rods only   FRP sheets only

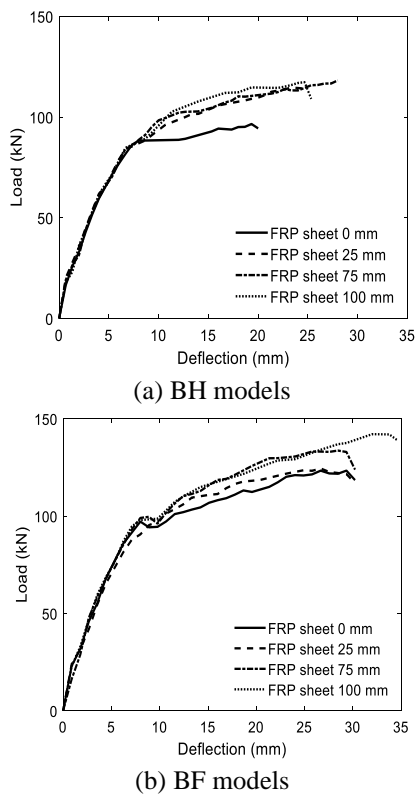Fig. 9 Schematic of the parametric study

(a) BH models

(b) BF models

Fig. 10 Response of load-deflection for strengthened beam models using several sizes of FRP sheets

a 3.38% disparity load while BH and BF had a 8.53% and 7.82% deviation load in terms of the ultimate load when compared with the numerical result.

4.3 Parametric study

The numerical FE model developed was used in the second part of this research to analyze the behavior of specimens which were not tested or produced using the experiment, and were not examined in the previous work by Haryanto *et al.* (2021b) that investigated the effect of FRP rods' diameters, compressive strength of concretes, ratio of steel reinforcement, as well as different types of the FRP rods on the flexural response and strength of the RC T-beams, particularly strengthened in the negative moment region with NSM half-embedded FRP rods. Four models were developed and analyzed to numerically determine the effect of varying the FRP sheet width and determine the contribution of FRP rods and sheets. Meanwhile, models without FRF rods or sheets were also developed and compared with other parametric models with the details discussed in the following sub-sections. Fig. 9 shows schematic of the parametric study.

4.3.1 Effect of FRP sheet width

The original FRP sheets in the experimental research were 100 mm wide with 30 mm spacing between each placed on the web of T-beams while its coverage was reported to be 72%. The parametric models were, therefore, designed with the use of 75 mm and 25 mm wide FRP sheets covering 54% and 18% respectively to achieve economic benefits. The effects of applying different FRP sheet widths in the FE model on the effectiveness of RC T-beams strengthened using FRP rods in the negative moment region are represented in Fig. 10. Meanwhile, the ultimate strength enhancement of the beams under different FRP sheet coverage of the models is presented in Fig 11. It was, however, discovered from Fig. 10 that an increment in the width of the FRP sheet increased the post-yielding stiffness for both BH and BF. This is important because post-yielding stiffness is one of the important variables associated with inelastic characteristics of structures affecting the dispersion of seismic response and a higher
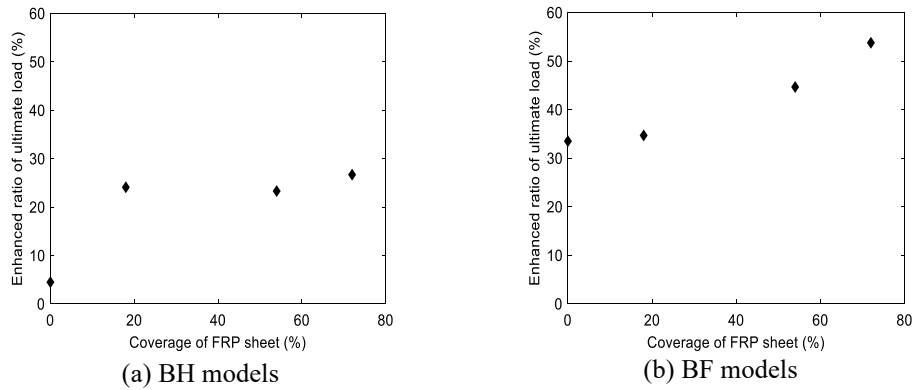
(a) BH models

(b) BF models

Fig. 11 Effect of FRP sheet sizes on the enhancement ratio of ultimate load

(a) Unstrengthened beam at 60 kN

(b) Only-FRP rods strengthened beam at 60 kN

(c) Only-FRP sheets strengthened beam at 60 kN

(a) Unstrengthened beam at 80 kN

(b) Only-FRP rods strengthened beam at 80 kN

(c) Only-FRP sheets strengthened beam at 80 kN

(a) Unstrengthened beam at 90 kN

(b) Only-FRP rods strengthened beam at 90 kN

(c) Only-FRP sheets strengthened beam at 90 kN
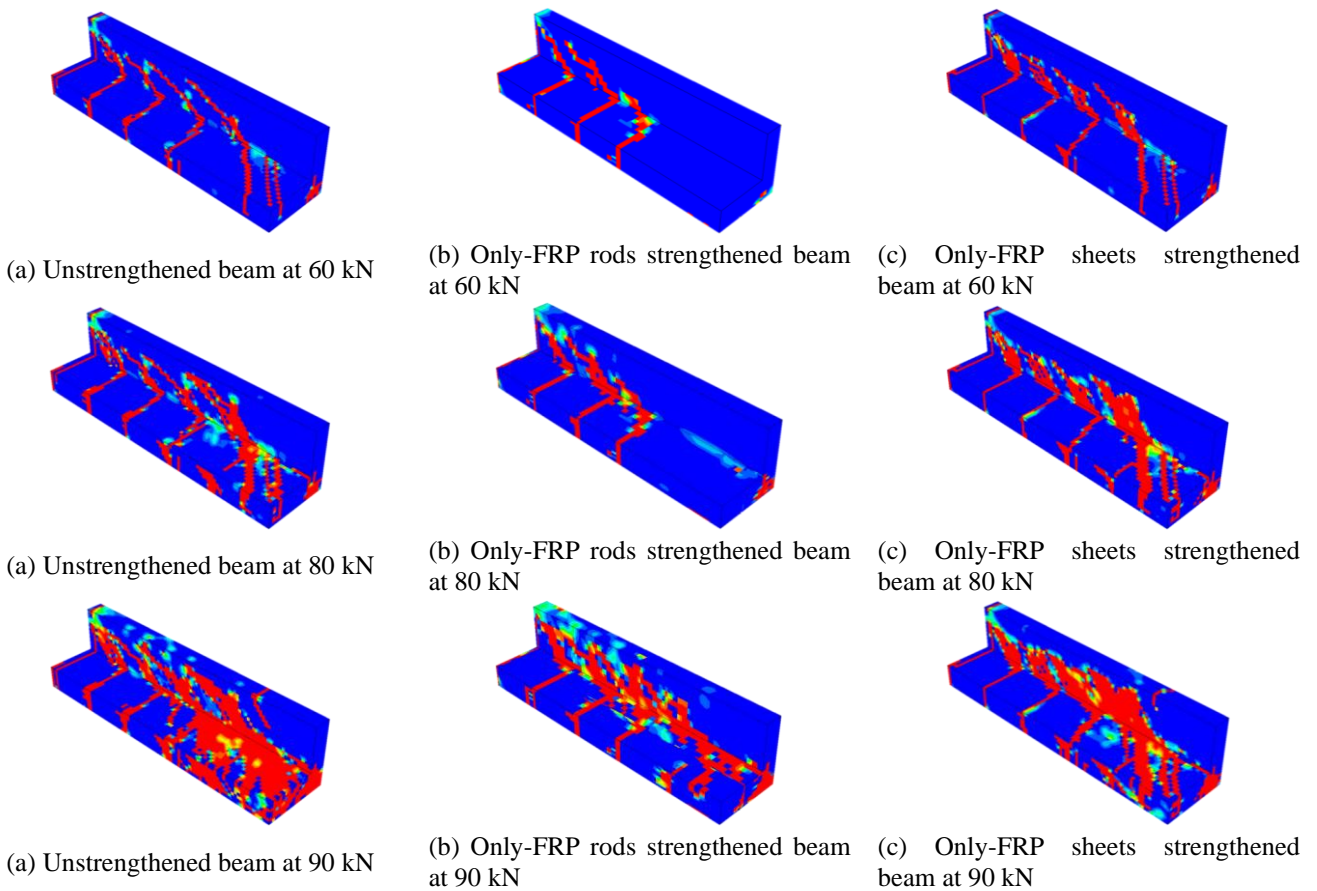
Fig. 12 Comparisons of tensile damage contours at different load

positive value for this parameter produces more uniform distribution of energy dissipation (Ye *et al.*2008).

Furthermore, Fig. 11 shows the ultimate load enhancement of only-FRP rods strengthened beam (FRP sheets 0% coverage) in BF models, which is 33.50%, is much higher than that of 4.50% in BH models. Also, Fig. 11 shows more FRP sheets coverage led to better ultimate load enhancement in BF and had slight effects in BH models. These findings indicated the presence of FRP sheets is effective for the improvement of beams' ultimate load either in BH or BF models while the width also has some influence. Therefore, an increment in FRP sheets coverage is recommended to ensure an effective increment in the beam's ultimate load.

4.3.2 Contribution of FRP rods and FRP sheets

The tensile damage contours for the monolithic beam which is the control specimen, only-FRP rods strengthened and half-embedded, and only-FRP sheets strengthened beam models at different load are shown in Fig. 12.

The tensile damage contour is represented by parameter d_t in the Concrete Damage Plasticity (CDP) model and is defined as the ratio of the cracking strain to the total strain. The red color in the contour shows d_t is close to 1 and this means tensile damage will occur. Fig. 12, however, shows the tensile damaged area of the beam at the support reduced

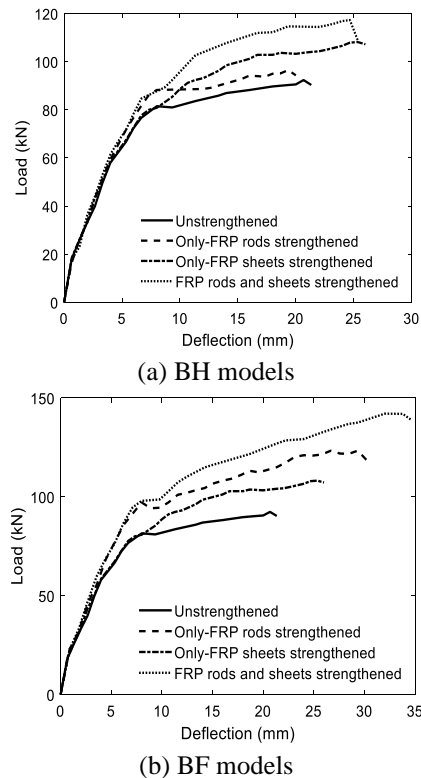(a) BH models

(b) BF models

Fig. 13 Contribution of FRP rods and sheets

under the same load after FRP rods reinforcement and this shows the material was effective in improving the beam's tensile strength at the bottom. Meanwhile, the FRP sheets reinforcement increased the tensile damaged area at the beam web along its own area and this indicates this material was able to uniformly transmit external forces to the beam web to limit the possibility of stress concentration problem in an unstrengthened beam.

Furthermore, the contribution of FRP rods and sheets on the performance of strengthened beams is shown in Fig. 13 with either observed to have a certain effect. However, the FRP rod was observed to be related to the strengthening of yield load while the FRP sheet is more related to the ductility of the specimen, apart from the ability of the FRPs to cause an increment in the ultimate load.

5. Conclusions

An FE numerical model was developed in this research to ensure the accurate simulation of the response to be provided by RC T-beams strengthened in the negative moment region through the use of NSM FRP rods and sheets as the shear reinforcement. The contact interaction between the surrounding materials and FRP rod through the use of cohesive behavior, nonlinearities in the compression and tension of the concrete material, steel reinforcement yielding ability, and FRP linearly elastic behavior were considered in the model. It was further used to predict the ultimate load of the beams placed under three-point bending and further validated through a comparison between numerical simulations for the FE and corresponding

experimental findings retrieved from three tests conducted in previous studies. Moreover, the effect of varying the width of the FRP sheet as well as the contributions of the FRP sheets and rods were examined on the performance of the specimens using a parametric study. The findings from this research are, therefore, presented as follows:

• A reasonable agreement was established concerning the response of load-deflection in all flexural loading stages up to when the specimens failed between the findings from the numerical simulations and the data provided by the experimental research.

• The analytical approach showed BH only had a 2.96% disparity load while BF had a 6.58% deviation load when compared with the numerical result.

• An increment in the width of the FRP sheets was found to have caused an increase in the post-yielding stiffness for both BH and BF and a higher stiffness usually produce more uniform distribution of energy dissipation.

• The tensile damaged area of the beam at the support reduced under the same load after FRP rods strengthening and this shows the material was effective in improving the beam's tensile strength at the bottom.

• The FRP sheets strengthening increased the tensile damaged area at the beam web along its own area and this indicates this material was able to uniformly transmit external forces to the beam web to limit the possibility of stress concentration problem in an unstrengthened beam.

• The FRP rods were observed to have more ability to strengthen yield load while FRP sheets focused more on the specimen ductility.

• The finite element model developed and validated in this research is considered appropriate to model and analyze RC T-beams which are strengthened in the negative moment region through the use of NSM FRP rods. It also has the ability to perform accurate and efficient parametric studies which are focused on designs of several configurations of strengthening using FRP materials.

• The findings of this study have to be seen in light of some limitations; FE mesh improvement should be addressed in the future research to avoid the localized crack formation.

Conflict of interest

The authors declare no potential conflict of interest.

Acknowledgments

References

Abdallah, M., Al Mahmoud, F., Khelil, A., Mercier, J. and Almassri, B. (2020), "Assessment of the flexural behavior of continuous RC beams strengthened with NSM-FRP bars, experimental and analytical study", *Compos. Struct.*, **242**, 112127. https://doi.org/10.1016/j.compstruct.2020.112127.

ACI Committee 318-14 (2014), Building Code Requirements for Structural Concrete and Commentary, American Concrete Institute, Farmington Hills, USA.

ACI Committee 440.2R-08 (2008), Guide for the Design and Construction of Externally Bonded FRP Systems for Strengthening Concrete Structures, American Concrete Institute, Farmington Hills, USA.

Al-Abdwaisab, A.H. and Al-Mahaidic, R.S. (2020), "Performance of reinforced concrete beams strengthened with NSM CFRP composites for flexure using cement-based adhesives", *Struct.*, **27**, 1446-1457. https://doi.org/10.1016/j.istruc.2020.07.047.

Al-Bayati, G., Al-Mahaidi, R. and Kalfat, R. (2016), "Experimental investigation into the use of NSM FRP to increase the torsional resistance of RC Beams using epoxy resins and cement-based adhesives", *Constr. Build. Mater.*, **124**, 1153-1164. https://doi.org/10.1016/j.conbuildmat.2016.08.095.

Al-Khafaji, A. and Salim, H. (2020), "Flexural strengthening of RC continuous T-beams using CFRP", *Fib.*, **8**(41), 1-18. https://doi.org/10.3390/fib8060041.

Al-Saadi, N.T.K., Mohammed, A., Al-Mahaidi, R. and Sanjayan, J. (2019), "A State-of-the-art review: Near-surface mounted FRP composites for reinforced concrete structures", *Constr. Build. Mater.*, **209**, 748-769. https://doi.org/10.1016/j.conbuildmat.2019.03.121.

Al-Saidya, A.H., Al-Harthya, A.S., Al-Jabria, K.S., Abdul-Halim, M. and Al-Shidi, N.M. (2010), "Structural performance of corroded RC beams repaired with CFRP sheets", *Compos. Struct.*, **92**(8), 1931-1938. https://doi.org/10.1016/j.compstruct.2010.01.001.

Alam, M.A., Jabbar, A.S.A., Jumaat, M. Z. and Mustapha, K.N. (2014), "Effective method of repairing RC beam using externally bonded steel plate", *Appl. Mech. Mater.*, **567**, 399-404. https://doi.org/10.4028/www.scientific.net/AMM.567.399.

Aldhafairi, F., Hassan, A., Abd-EL-Hafez, L.M. and Abouelezz, A.E.Y. (2020), "Different techniques of steel jacketing for retrofitting of different types of concrete beams after elevated temperature exposure", *Struct.*, **28**, 713-725. https://doi.org/10.1016/j.istruc.2020.09.017.

Almassri, B. and Halahla, A.M. (2020), "Corroded RC beam repaired in flexure using NSM CFRP rod and an external steel plate", *Struct.*, **27**, 343-351. https://doi.org/10.1016/j.istruc.2020.05.054.

Asplund, S.O. (1949), "Strengthening bridge slabs with grouted reinforcement", *J. Am. Concrete Inst.*, **20**(6), 397-406.

Attar, H.S., Esfahani, M.R. and Ramezani, A. (2020), "Experimental investigation of flexural and shear strengthening of RC beams using fiber-reinforced self-consolidating concrete jackets", *Struct.*, **27**, 46-53. https://doi.org/10.1016/j.istruc.2020.05.032.

Barris, C., Sala, P., Gómez, J. and Torres, L. (2020), "Flexural behaviour of FRP reinforced concrete beams strengthened with NSM CFRP strips", *Compos. Struct.*, **241**, 112059. https://doi.org/10.1016/j.compstruct.2020.112059.

Belarbi, A. and Thomas, T.C. (1994), "Constitutive laws of concrete in tension and reinforcing bars stiffened by concrete", *ACI Struct. J.*, **91**(4), 465-474. https://doi.org/10.14359/4154.

Budipriyanto, A., Han, A.L. and Hu, H.T. (2018), "Bond-shear behavior of FRP rods as a function of attachment configuration", *J. Adv. Res. Civil Environ. Eng.*, **1**(1), 9-17. http://doi.org/10.30659/jacee.1.1.9-17.

Chellapandian, M., Prakash, S.S. and Sharma, A. (2018), "Experimental and finite element studies on the flexural behavior of reinforced concrete elements strengthened with hybrid FRP technique", *Compos. Struct.*, **208**, 466-478. https://doi.org/10.1016/j.compstruct.2018.10.028.

Chen, C., Wang, X. and Cheng, L. (2019), "Modeling NSM FRP strengthened RC beams under fatigue due to IC-debonding", *Int. J. Fatigue.*, **126**, 174-187. https://doi.org/10.1016/j.ijfatigue.2019.04.039.

Chen, C.C. and Tseng, C.L. (2001), "Ductility Enhancement of RC beams confined by steel cover plates", *J. Chin. Inst. Eng.*, **24**(1), 55-64. http://doi.org/10.1080/02533839.2001.9670606.

Construction Agency (2019), General Rules for Revision of Design Code for Concrete Structures, Ministry of Interior, Taipei, Taiwan.

Cosenza, E., Manfredi, G. and Realfonzo, R. (1997), "Behavior and modeling of bond of FRP rebars to concrete", *J. Compos. Constr.*, **1**(2), 40-51. https://doi.org/10.1061/(ASCE)1090-0268(1997)1:2(40).

De Lorenzis, L. and Teng, J.G. (2007), "Near-surface mounted FRP Reinforcement: an emerging technique for strengthening structures", *Compos. B. Eng.*, **38**(2), 119-143. https://doi.org/10.1016/j.compositesb.2006.08.003.

Deng, Y., Li, Z., Zhang, H., Corigliano, A., Lam, A.C.C., Hansapinyo, C. and Yan, Z. (2021a), "Experimental and analytical investigation on flexural behaviour of RC beams strengthened with NSM CFRP prestressed concrete prisms", *Compos. Struct.*, **257**, 113385. https://doi.org/10.1016/j.compstruct.2020.113385.

Deng, Y., Ma, F., Zhang, H., Wong, S.H.F., Pankaj, P., Zhu, L., Ding, L. and Bahadori-Jahromi, A. (2021b), "Experimental study on shear performance of RC beams strengthened with NSM CFRP prestressed concrete prisms", *Eng. Struct.*, **235**, 112004. https://doi.org/10.1016/j.engstruct.2021.112004.

Firmo, J.P., Arruda, M.R.T, Correia, J.R. and Rosa, I.C. (2018), "Three-dimensional finite element modelling of the fire behaviour of insulated RC beams strengthened with EBR and NSM CFRP strips", *Compos. Struct.*, **183**, 124-136. https://doi.org/10.1016/j.compstruct.2017.01.082.

Haryanto, Y., Gan, B.S. and Maryoto, A. (2017a), "Wire rope flexural bonded strengthening system on RC-beams: A finite element simulation", *Int. J. Tech.*, **8**(1), 134-144. https://doi.org/10.14716/ijtech.v8i1.2734.

Haryanto, Y., Gan, B.S., Widyaningrum, A. and Maryoto, A. (2017b), "Near surface mounted bamboo reinforcement for flexural strengthening of reinforced concrete beams", *J. Teknologi*, **79**(6), 233-240. https://doi.org/10.11113/jt.v79.10767.

Haryanto, Y., Gan, B.S., Widyaningrum, A., Wariyatno, N.G. and Fadli, A. (2018), "On the performance of steel wire rope as the external strengthening of RC beams with different end-anchor type", *J. Teknologi*, **80**(5), 145-154. https://doi.org/10.11113/jt.v80.11588.

Haryanto, Y., Han, A.L., Hu, H.T., Hsiao, F.P., Hidayat, B.A. and Widyaningrum A. (2021a), "Enhancement of flexural performance of RC beams with steel wire rope by external strengthening technique", *J. Chin. Inst. Eng.*, **44**(3), 193-203. https://doi.org/10.1080/02533839.2021.1871651.

Haryanto, Y., Hu, H.T., Han, A.L, Atmajayanti, A.T., Galuh, D.L.C. and Hidayat, B.A. (2019), "Finite element analysis of T-section RC beams strengthened by wire rope in the negative moment region with an addition of steel rebar at the compression block", *J. Teknologi*, **81**(4), 143-154. https://doi.org/10.11113/jt.v81.12974.

Haryanto, Y., Hu, H.T., Han, A.L., Hsiao, F.P., Teng, C.J., Hidayat, B.A. and Wariyatno, N.G. (2021b), "Negative moment region flexural strengthening system of RC T-beams with half-

embedded NSM FRP rods: a parametric analytical approach", *J. Chin. Inst. Eng.*, **44**(6), 553-561. https://doi.org/10.1080/02533839.2021.1936646.

Haryanto, Y., Hu, H.T., Han, A.L., Hsiao, F.P., Teng, C.J., Hidayat, B.A. and Nugroho, L. (2021c), "Nonlinear 3D model of double shear lap tests for the bond of near-surface mounted FRP rods in concrete considering different embedment depth", *Period. Polytech. Civil Eng.*, **65**(3), 878-889. https://doi.org/10.3311/PPci.17309.

Hawileh, R.A. (2012), "Nonlinear finite element modeling of RC beams strengthened with NSM FRP rods", *Constr. Build. Mater.*, **27**(1), 461-471. https://doi.org/10.1016/j.conbuildmat.2011.07.018.

Hidayat, B.A., Hu, H.T., Han, A.L., Haryanto, Y., Widianingrum, A. and Pamudji, G. (2019), "Nonlinear finite element analysis of traditional flexural strengthening using betung bamboo (Dendrocalamus asper) on concrete beams", *IOP Conf. Ser. Mater. Sci. Eng.*, **615**, 012073. https://doi.org/10.1088/1757-899X/615/1/012073.

Hsu, L.S and Hsu, C.T.T. (1994), "Complete stress-strain behaviour of high-strength concrete under compression", *Mag. Concrete Res.*, **46**(169), 301-312. https://doi.org/10.1680/macr.1994.46.169.301.

Hu, H.T., Lin, F.M. and Jan, Y.Y. (2004), "Nonlinear finite element analysis of reinforced concrete beams strengthened by fiber-reinforced plastics", *Compos. Struct.*, **63**(3-4), 271-281. https://doi.org/10.1016/S0263-8223(03)00174-0.

Hung, C.C., Prasetya, B.H. and Han, A.L. (2020), "The behavior of reinforced concrete members with section enlargement using self-compacting concrete", *Int. Rev. Civil Eng.*, **11**(3), 121-126. https://doi.org/10.15866/irece.v11i3.18574.

Hwang, Y.H., Yang, K.H., Mun, J.H. and Kwon, S.J. (2020), "Axial performance of RC columns strengthened with different jacketing methods", *Eng. Struct.*, **206**, 110179. https://doi.org/10.1016/j.engstruct.2020.110179.

Jumaat, M.Z., Rahman, M.M. and Alam, M.A. (2010), "Flexural strengthening of RC continuous T beam using CFRP laminate: A review", *Int. J. Phys. Sci.*, **5**(6), 619-625. https://doi.org/10.5897/IJPS.9000263.

Kaplan, H., Yilmaz, S., Cetinkaya, N. and Atimtay, E. (2011), "Seismic strengthening of RC structures with exterior shear walls", *Sadhana*, **36**(17), 17-34. https://doi.org/10.1007/s12046-011-0002-z.

Lee, S.H., Shin, K.J. and Lee, H.D. (2018), "Post-tensioning steel rod system for flexural strengthening in damaged reinforced concrete (RC) beams", *Appl. Sci.*, **8**(10), 1763. https://doi.org/10.3390/app8101763.

Lesmana, C., Hu, H.T., Lin, F.M. and Huang, N.M. (2013), "Numerical analysis of square reinforced concrete plates strengthened by fiber-reinforced plastics with various patterns", *Compos. B. Eng.*, **55**, 247-262. https://doi.org/10.1016/j.compositesb.2013.06.021.

Lin, C.T., Wu, Y.H., Chin, W.H. and Lin, M.L. (2014), "Performance of CFRP-strengthened RC beams subjected to repeated loads", *J. Chin. Inst. Eng.*, **37**(8), 1007-1017. http://doi.org/10.1080/02533839.2014.912778.

National Standardization Agency of Indonesia (2017), Concrete Steel Reinforcement, National Standardization Agency of Indonesia, Jakarta, Indonesia.

Nie, X.F., Zhang, S.S., Chen, G.M. and Yu, T. (2020), "Strengthening of RC beams with rectangular web openings using externally bonded FRP: numerical simulation", *Compos. Struct.*, **248**, 112552. https://doi.org/10.1016/j.compstruct.2020.112552.

Nuroji, Hung, C.C., Prasetya, B.H. and Han, A.L. (2020), "The behavior of reinforced concrete members with section enlargement using self-compacting concrete", *Int. Rev. Civil*

Eng., **11**(3), 121-126. https://doi.org/10.15866/irece.v11i3.18574.

Parvin, A. and Shah, T.S. (2016), "Fiber reinforced polymer strengthening of structures by near-surface mounting method", *Polym.*, **8**(8), 298. https://doi.org/10.3390/polym8080298.

Sabau, C., Popescu, C., Sas, G., Schmidt, J.W., Blanksvärd, T. and Täljsten, B. (2018), "Strengthening of RC beams using bottom and side NSM reinforcement", *Compos. B. Eng.*, **149**, 82-91. https://doi.org/10.1016/j.compositesb.2018.05.011.

Salama, A.S.D., Hawileh, R.A. and Abdalla, J.A. (2019), "Performance of externally strengthened RC beams with side-bonded CFRP sheets", *Compos. Struct.*, **212**, 281-290. https://doi.org/10.1016/j.compstruct.2019.01.045.

Sapulete, C.A. (2018), "Experimental study on the effect of FRP rods and wrap as a flexural strengthening on the RC beams", Master Thesis, Diponegoro University.

Sharaky, I.A., Baena, M., Barris, C., Sallam, H.E.M. and Torres, L. (2018), "Effect of axial stiffness of NSM FRP reinforcement and concrete cover confinement on flexural behaviour of strengthened RC beams: Experimental and numerical study", *Eng. Struct.*, **173**, 987-1001. https://doi.org/10.1016/j.engstruct.2018.07.062.

Sharaky, I.A., Reda, R.M., Ghanem, M., Seleem, M.H. and Sallam, H.E.M. (2017), "Experimental and numerical study of RC Beams Strengthened with Bottom and Side NSM GFRP bars having different end conditions", *Constr. Build. Mater.*, **149**, 882-903. https://doi.org/10.1016/j.conbuildmat.2017.05.192.

Sharaky, I.A., Torres, L. and Sallam, H.E.M. (2015), "Experimental and analytical investigation into the flexural performance of RC beams with partially and fully bonded NSM FRP bars/strips", *Compos. Struct.*, **122**, 113-126. https://doi.org/10.1016/j.compstruct.2014.11.057.

Sharaky, I.A., Torres, L., Baena, M. and Miàs, C. (2013), "An experimental study of different factors affecting the bond of NSM FRP bars in concrete", *Compos. Struct.*, **99**, 350-365. https://doi.org/10.1016/j.compstruct.2012.12.014.

Sherwood, E.G. and Soudki, K.A. (2000), "Rehabilitation of corrosion damaged concrete beams with CFRP laminates-a pilot study", *Compos. B. Eng.*, **31**(6-7), 453-459. https://doi.org/10.1016/S1359-8368(99)00043-8.

Simulia (2007), Abaqus Technology Brief Projectile Impact on a Carbon Fiber Reinforced Plate, Abaqus Technology Brief.

Stoner, J.G. and Polak, M.A. (2020), "Finite element modelling of GFRP reinforced concrete beams", *Comput. Concrete*, **25**(4), 369-382. http://doi.org/10.12989/cac.2020.25.4.369.

Systemes D. (2011), Dassault Systemes, Rhode Island, USA.

Täljsten, B. and Elfgren, L. (2000), "Strengthening concrete beams for shear using CFRP-materials: Evaluation of different application methods", *Compos. B. Eng.*, **31**(2), 87-96. https://doi.org/10.1016/S1359-8368(99)00077-3.

Tan, K.H. (2014), "Beam strengthening by external post-tensioning: design recommendations", *IES J. Part A: Civil Struct. Eng.*, **7**(4), 219-228. http://doi.org/10.1080/19373260.2014.947086.

Tsai, S.W. and Wu, E.M. (1971), "A general theory of strength for anisotropic materials", *J. Compos. Mater.*, **5**(1), 58-80. https://doi.org/10.1177/002199837100500106.

Tudjono, S., Han, A.L. and Gan, B.S. (2017), "Revitalization of cracked flexural members using retrofitting and synthetic wrapping", *Proc. Eng.*, **171**, 1123-1128. https://doi.org/10.1016/j.proeng.2017.01.472.

Tudjono, S., Han, A.L. and Gan, B.S. (2018), "An integrated system for enhancing flexural members' capacity via combinations of the fiber reinforced plastic use, retrofitting, and surface treatment techniques", *Int. J. Tech.*, **9**(1), 5-15. https://doi.org/10.14716/ijtech.v9i1.298.

Tudjono, S., Han, A.L. and Hidayat, B.A. (2015), "An

experimental study to the influence of fiber reinforced polymer (FRP) confinement on beams subjected to bending and shear", *Proc. Eng.*, **125**, 1070-1075. https://doi.org/10.1016/j.proeng.2015.11.164.

Wang, Q., Zhu, H., Li, T., Wu, G. and Hu, X. (2019), "Bond performance of NSM FRP bars in concrete with an innovative additional ribs anchorage system: an experimental study", *Constr. Build. Mater.*, **207**, 572-584. https://doi.org/10.1016/j.conbuildmat.2019.02.020.

Wei, L., Ming, X. and Zhongfan, C. (2014), "Parameters calibration and verification of concrete damage plasticity model of ABAQUS", *Ind. Constr.*, **44**(S1), 167-171.

Xue, W., Tan, Y. and Zeng, L. (2010), "Flexural response predictions of reinforced concrete beams strengthened with prestressed CFRP plates", *Compos. Struct.*, **92**(3), 612-622. https://doi.org/10.1016/j.compstruct.2009.09.036.

Yang. Y., Fahmy, M.F.M., Cui, J., Pan, Z. and Shie, J. (2019), "Nonlinear behavior analysis of flexural strengthening of RC beams with NSM FRP laminates", *Struct.*, **20**, 374-384. https://doi.org/10.1016/j.istruc.2019.05.001.

Ye, L.P., Lu, X.Z., Ma, Q.L., Cheng, G.Y., Song, S.Y., Miao, Z.W. and Pan, P. (2008), "Study on the influence of post-yielding stiffness to the seismic response of building structures", *Proceedings of the 14th World Conference on Earthquake Engineering*, Beijing, October.

Zhang, S.S. and Teng, J.G. (2014), "Finite element analysis of end cover separation in RC beams strengthened in flexure with FRP", *Eng. Struct.*, **75**, 550-560. https://doi.org/10.1016/j.engstruct.2014.06.031.

Zhang, X., Luo, Y., Wang, L., Zhang, J., Wu, W. and Yang, C. (2018), "Flexural strengthening of damaged RC T-beams using self-compacting concrete jacketing under different sustaining load", *Constr. Build. Mater.*, **172**, 185-195. https://doi.org/10.1016/j.conbuildmat.2018.03.245.

JK